NJC

PAPER

View Article Online
View Journal

Cite this: DOI: 10.1039/c8nj00537k

Competition between hydrogen bonds and halogen bonds: a structural study†

Janaka C. Gamekkanda,[a] Abhijeet S. Sinha,[a] John Desper,[a] Marijana Đaković[b] and Christer B. Aakeröy*[a]

The competition and balance between intermolecular hydrogen bonds (HBs) and halogen bonds (XBs) were explored by co-crystallizing tetra-functionalized (2 × HB (–OH) and 2 × XB (–C≡C–I)) molecules, *trans*-1,4-bis(iodoethynyl)cyclohexane-1,4-diol (**D1**) and *cis*-1,4-bis(iodoethynyl)cyclohexane-1,4-diol (**D2**), with six ditopic nitrogen based acceptor molecules. The crystal structures of both **D1** and **D2** showed non-covalent interactions between HB/XB donors and available acceptor sites (oxygen/triple bond/negative region of iodine). In three co-crystals of **D1** the HB and XB donors act in similar ways as both activated iodine and hydroxyl hydrogen bind to the nitrogen acceptors in the solid state. In contrast, in a co-crystal of **D2**, a geometric isomer of **D1**, there were only hydrogen bonds to the co-former and the halogen-bond donor interacted with the hydroxyl oxygen atoms of **D2**. A stronger tendency for linear XB interactions (as well as greater van der Waals radii reduction) was observed with nitrogen atoms as acceptors (average reduction = 21%) compared to those involving an oxygen atom as an acceptor (average reduction = 16%). A control molecule, *trans*-1,4-diethynylcyclohexane-1,4-diol (**D3**), which has only HB donors (–OH and –C≡C–H) was also examined to get a better understanding of the balance between XB and HB intercations. The ethynyl hydrogen atom did not form hydrogen bonds to the nitrogen atoms in acceptors, and only O–H···N and –C≡C–H···O hydrogen bonds were observed in these structures.

Received 30th January 2018,
Accepted 13th April 2018

DOI: 10.1039/c8nj00537k

rsc.li/njc

In order to develop practical and robust strategies for the efficient synthesis of co-crystals,[1] it is helpful to employ intermolecular interactions that can provide a hierarchical assembly protocol.[2,3] By combining interactions that do not compete for the same molecular binding sites it is, in principle, possible to avoid or at least minimize "synthon cross-over"[4] thereby producing architectures of considerable complexity.[5–8] For some time, hydrogen bonds (HB) were the preeminent synthetic tool in this arena,[9–12] but halogen bonds (XB) have also received much attention as a vehicle for the synthesis and directed assembly of supramolecular heteromeric architectures.[13–18] Both interactions are directional and relatively strong, and their importance in crystal engineering originates from their shared dependence upon long-range electrostatic forces.[19–23] Interestingly, several cases of solid-state HB/XB mimicry have been reported where an acceptor site (electron-pair donor) forms structurally identical interactions with both HB and XB donors.[24] For example, a hydrogen-bond donor hydroquinone plays the same supramolecular role when interacting with 4,4′-bipyridine[25] as iodine, 1,4-diiodobenzene,[26] and 1,4-diiodo-tetrafluorobenzene,[27] respectively. Structurally similar interactions are found in the co-crystals of tetramethylpyrazine with both 1,4-diiodotetrafluorobenzene[28] and hydroquinone,[29] and aminopyrimidine-based ethynyl and iodoethynyl donors form equivalent architectures with tetramethylpyrazine and 1,2-bis(4-pyridyl)ethylene.[30] A small number of studies have also explored the competition between these interactions through experimental[31–33] and theoretical[34] means, by affixing a HB and an XB donor on the same molecular backbone. In addition, the competition between separate XB and HB donors for the same acceptor, *e.g.* mixtures of 1,2-bis(4-pyridyl)ethane, 1,4-diiodotetrafluorobenzene and hydroquinone,[27] or of *N*,*N*,*N*′,*N*′-tetramethylethylenediamine, 1,2-diiodo-tetrafluoroethane and ethylene glycol,[27] or bi-functional molecules including 4-iodotetrafluorobenzoic acid, 4-iodotetrafluorophenol and 4-iodotetrafluoroaldoxime with acceptors such as 4,4′-azobipyridine,[35] have been reported. The fact that hydrogen bonding and halogen bonding have shared origins suggests that if we are to advance supramolecular synthesis, we need to learn more about the balance between them in systems where they are likely to compete for the same acceptor sites.

The strength of an XB donor can be enhanced through the addition of electron-withdrawing substituents, but a similar effect can also be achieved by positioning the halogen atom

---

[a] *Department of Chemistry, Kansas State University, Manhattan, KS, 66506, USA. E-mail: aakeroy@ksu.edu*

[b] *Department of Chemistry, Faculty of Science, University of Zagreb, Horvatovac 102a, HR-10000 Zagreb, Croatia*

† Electronic supplementary information (ESI) available. CCDC 1820020–1820028. TGA, DSC, and crystallographic data. For ESI and crystallographic data in CIF or other electronic format see DOI: 10.1039/c8nj00537k

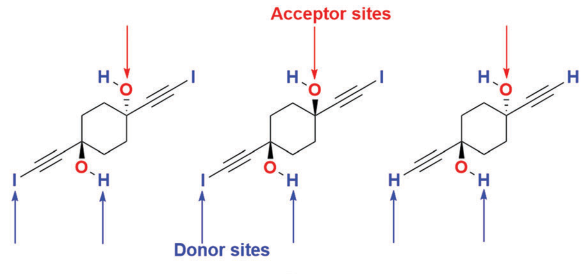

Scheme 1 Probe molecules with competing halogen- and hydrogen-bond donors (**D1**/**D2**) and competing hydrogen-bond donors (**D3**).

next to an sp-hybridized carbon atom.[26,36] Despite the increasing popularity of this route for creating powerful XB donors,[37] only a limited amount of work has been done on the potential competition between such XB donors and HB donors. To remedy this lack of experimental data, we synthesized two tetra-functionalized molecules and subjected them to co-crystallization experiments with six different acceptors; *trans*-1,4-bis(iodoethynyl)cyclohexane-1,4-diol (**D1**) and *cis*-1,4-bis(iodoethynyl)cyclohexane-1,4-diol (**D2**) which are geometric isomers of each other and are equipped with two HB and two XB donors, respectively, Scheme 1. In addition, we also explored the structural chemistry of *trans*-1,4-diethynylcyclohexane-1,4-diol (**D3**) which has two pairs of competing HB donors on the same cyclohexane framework.

The XB donors in **D1**/**D2** are ''activated'' by an sp-hybridized carbon atom, and **D3** acts as a control molecule where the XB donor, R–C≡C–I, has been replaced with a geometrically identical HB donor, R–C≡C–H. Two different isomers of the XB donor (*trans*/*cis*) were prepared in order to explore whether/how molecular geometry would affect synthon preferences. All six acceptor molecules in this study were symmetric ditopic N-heterocyclic compounds, Scheme 2.

Given the specific combination of donor and acceptor molecules investigated herein, we hypothesised a series of different outcomes if **D1–D3** were to form co-crystals with N-heterocyclic acceptors **A1–A6**, Schemes 3 and 4.

By having the competing halogen- and hydrogen-bond donors on the same molecular backbone, the results will not be affected by potential solubility differences which could come into play if the donors were residing on different molecules.

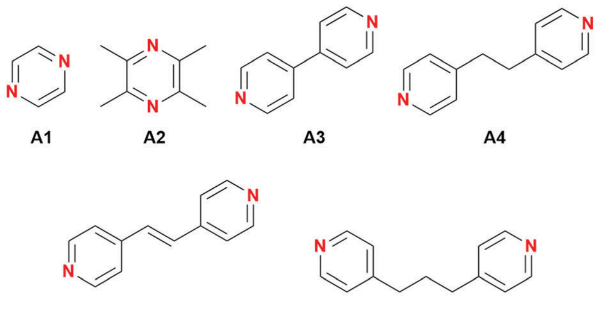

Scheme 2 Six ditopic XB and HB acceptors.

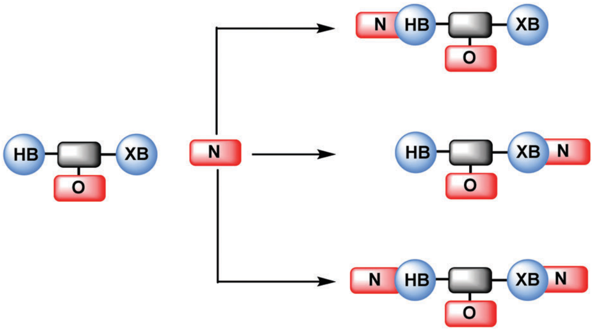

Scheme 3 Postulated primary intermolecular interactions in co-crystals of **D1**/**D2**:**A1–A6**.

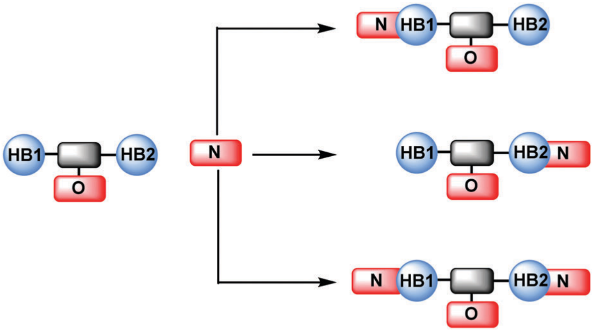

Scheme 4 Postulated intermolecular interactions in co-crystals of **D3**:**A1–A6**.

Since both XB and HB interactions are dependent upon electrostatic features, we complemented the structural study with an analysis of calculated molecular electrostatic potential surfaces for **D1–D3** in order to try rationalise the outcome of co-crystallizations. Through these complementary approaches we hoped to shed more light on the supramolecular competition and balance between the two most common synthetic tools in current crystal engineering.

Experimental section

Materials and methods

All solvents, reagents, precursors and acceptors (**A1–A6**) were purchased from commercial sources and used without further purification. Melting points were determined using a Fisher-Johns melting point apparatus and are uncorrected. Infrared spectra were recorded on a Nicolet 380 FT-IR spectrometer (optical resolution $<0.9\ \text{cm}^{-1}$). ^{1}H NMR spectra were recorded on a Varian unity plus 400 MHz spectrometer. DSC data were obtained on a TA instruments Q20 and TGA data on a TA instruments Q50.

Computational studies

Starting geometries of the molecules were obtained using the Merck Molecular Mechanics Force Field. All subsequent calculations were carried out using the B3LYP functional and 6-31G* basis set which employs LANL2DZ[38] under vacuum in Spartan'14 software.[39] Molecular electrostatic potential surfaces were generated for the optimized structures on the electron isodensity surface of 0.002 electrons per a.u.[3]

Synthesis of D1–D3. The three donors were synthesized using commercially available 1,4-cyclohexanedione. The ketone was converted to propargyl alcohol with a TMS protected alkyne group[40] (*trans*-cyclohexane being the major product). **D3** was obtained by deprotecting the ethynyl group and **D1** and **D2** were obtained by a reaction with *N*-iodosuccinimide, Scheme 5.

Synthesis of *trans*- and *cis*-1,4-bis((trimethylsilyl)ethynyl)-cyclohexane-1,4-diol. A solution of trimethylsilylacetylene (1.75 ml, 18 mmol) was stirred in 100 ml of dry THF and cooled to −10 °C under N$_2$. A solution of *n*-BuLi (4.9 ml 18 mmol) was added slowly over 30 min at −10 °C under N$_2$. The mixture was stirred for an additional hour at the same temperature. Cyclohexane-1,4-dione (1.0 g, 8.9 mmol) was dissolved in 25 ml of dry THF and added dropwise to the resulting trimethylsilyl acetylide solution under N$_2$ at −10 °C. The mixture was then allowed to reach room temperature and stirred overnight. After completion of the reaction, 100 ml of water was added and the mixture was extracted with ethyl acetate (3 × 100 ml). The combined organic layers were dried over magnesium sulfate and the solution was concentrated to obtain a crude solid and purified by column chromatography. The *trans* isomer was obtained using hexane as the eluent and the *cis* isomer was obtained using a mixture of hexanes: ethyl acetate (8 : 2) as the eluent. Yield: *trans* isomer 1.43 g, 52%, m.p.: 160–163 °C, ^{1}H NMR (400 MHz in DMSO-d6): 5.43 (2H, s), 1.77–1.62 (8H, m), 0.13 (18H, s); *cis* isomer 0.410 g, 15%, m.p.: 123–125 °C, ^{1}H NMR (400 MHz in DMSO-d6): 5.31 (2H, s), 1.71–1.68 (8H, m), 0.12 (18H, s).

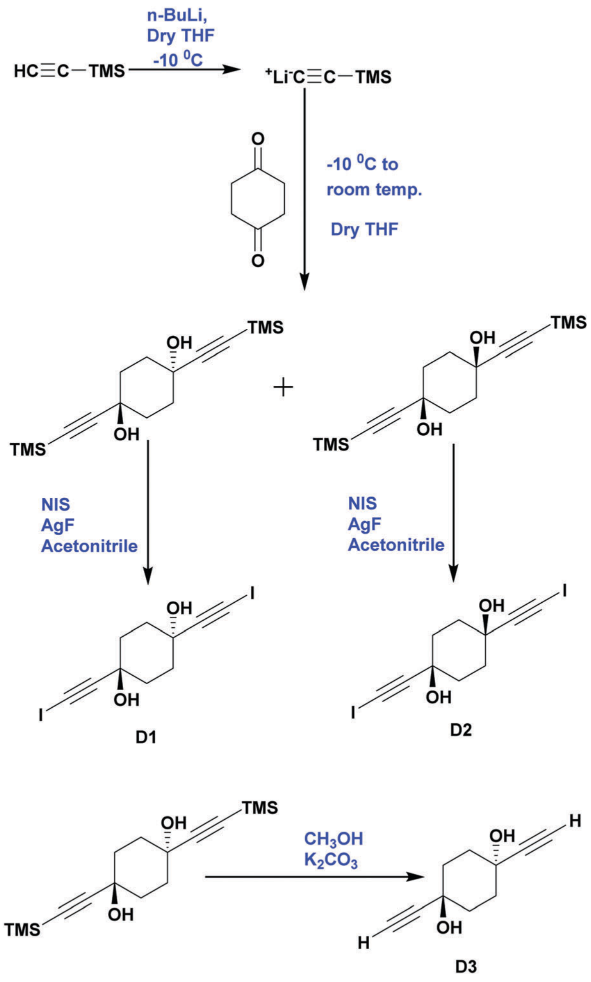

Scheme 5 Overview of the synthesis of **D1–D3**.

Synthesis of *trans*-1,4-bis(iodoethynyl)cyclohexane-1,4-diol·H$_2$O (D1·H$_2$O). Silver fluoride (0.825 g, 6.5 mmol) and *trans*-1,4-bis((trimethylsilyl)ethynyl)cyclohexane-1,4-diol (1.0 g, 3.24 mmol) were dissolved in 50 ml of acetonitrile and N$_2$ was bubbled through the solution for 20 minutes. *N*-Iodosuccinimide (1.46 g, 6.5 mmol) was added to the mixture and the flask was covered with aluminum foil. The reaction mixture was stirred overnight under N$_2$. After completion of the reaction, the resulting mixture was passed through a short pad of silica and the resulting solution was evaporated under vacuum in order to get the crude product. It was dissolved in methanol and water was added to the mixture. The product crashed out and the precipitate was filtered and dried in air to give a light-yellow solid. Yield 1.23 g, 87%, m.p.: 218–220 °C (dec.), ^{1}H NMR (400 MHz in DMSO-d6): 5.49 (2H, s), 1.75–1.57 (8H, m).

Synthesis of *cis*-1,4-bis(iodoethynyl)cyclohexane-1,4-diol (D2). The synthesis of *cis*-1,4-bis(iodoethynyl)cyclohexane-1,4-diol was carried out in the same way as the synthesis of **D1** by using 0.250 g (2.0 mmol) of silver fluoride, and 0.3 g (0.97 mmol) of *cis*-1,4-bis((trimethylsilyl)ethynyl)cyclohexane-1,4-diol and 0.450 g (2.0 mmol) of *N*-iodosuccinimide dissolved in 30 ml of acetonitrile. Yield: 0.360 g, 89%, m.p.: 168–171 °C (dec.), ^{1}H NMR (400 MHz in DMSO-d6): 5.40 (2H, s), 1.71–1.61 (8H, m).

Synthesis of *trans*-1,4-diethynylcyclohexane-1,4-diol·H$_2$O (D3·H$_2$O). *trans*-1,4-Bis((trimethylsilyl)ethynyl)cyclohexane-1,4-diol (0.5 g, 1.6 mmol) and potassium carbonate (0.45 g, 3.25 mmol) were dissolved in 50 ml of methanol. The reaction mixture was stirred for 4 h and after completion of the reaction, the solvent was evaporated under vacuum. The solid mixture was dissolved in ethyl acetate and washed with brine. The organic layer was dried over magnesium sulfate and the solvent was evaporated to get a white powder as the product. Yield 0.22 g, 75%, m.p.: 175–178 °C, ^{1}H NMR (400 MHz in DMSO-d6): 5.41 (2H, s), 3.28 (2H, s), 1.79–1.64 (8H, m).

Crystal growth of D1–D3 and synthesis of co-crystals. **D1–D3** (10 mg) were individually dissolved in methanol (2 ml) and kept in small vials at room temperature to get single crystals. Eighteen experiments were performed and the resulting solids were analysed using IR spectroscopy. The solid mixtures obtained from the grinding experiments were dissolved in 2 ml of methanol or methanol/tetrahydrofuran and kept in small vials for slow evaporation at room temperature. Crystals suitable for single-crystal X-ray diffraction were obtained after 2–3 days.

Results

D1 and **D3** crystallized as monohydrates, whereas **D2** did not include any solvent in its lattice. These results were confirmed by TGA, which show the loss of one equivalent of water for both **D1** and **D3** (but not for **D2**), and by DSC, which indicate

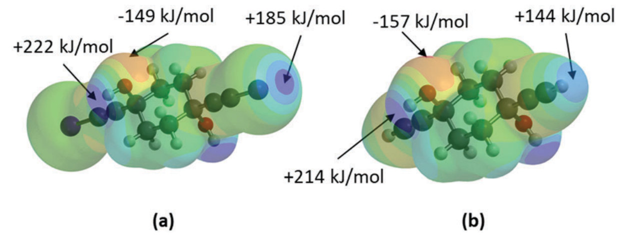

Fig. 1 Electrostatic potential surfaces of (a) XB/HB donors and acceptors of **D1**, (b) HB donors and acceptors of **D3**.

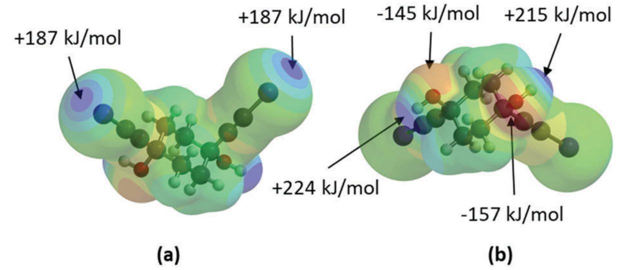

Fig. 2 Electrostatic potential surfaces of (a) XB donors, (b) HB donors and XB/HB acceptors of **D2**.

thermodynamic events at matching temperatures for **D1** and **D3** (ESI†).

The relevant maximum positive and negative values on the electrostatic potential surfaces for **D1** and **D3** are listed in Fig. 1(a) and (b), respectively, for **D2** they are listed in Fig. 2.

MEPs of **A1–A6** were calculated in order to rank the ability of these molecules to act as HB/XB acceptors (Fig. 3).

D1–D3 and six co-crystals thereof produced crystals suitable for single-crystal X-ray diffraction, and the crystallographic data are provided in the ESI.† Atomic displacement parameters (ADPs) and labelling schemes for all crystal structures are shown in Fig. 4.

Geometric parameters for hydrogen and halogen bonds in the crystal structures of **D1–D3** are given in Tables 1 and 2, respectively.

All four donors on **D1** (2 × O–H and 2 × R–C≡C–I) are involved in intermolecular interactions. The intermolecular network becomes more complicated by the presence of a water molecule in the lattice. Both XB donors interact with –OH groups of **D1** in a homomeric manner, whereas the hydroxylic HB donors bind to the oxygen atom of water. The disordered water molecule acts as a hydrogen bond donor to the hydroxylic oxygen atoms of **D1**, Fig. 5.

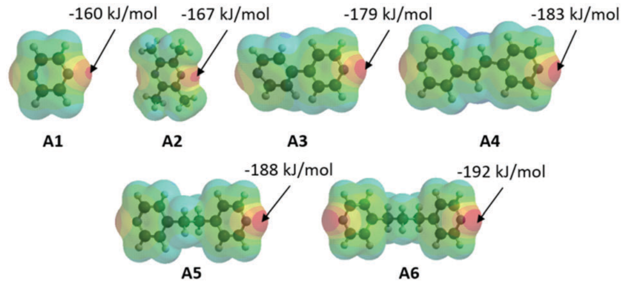

Fig. 3 Electrostatic potential surfaces of acceptor atoms in **A1–A6**.

In the crystal structure of **D2**, there are two intermolecular hydrogen bonds between adjacent hydroxyl groups (Fig. 6a). In addition, there is one XB involving the triple bond of **D2** as an acceptor site *r*(I···centroid of the triple bond) *ca.* 3.27 Å, *θ*(centroid of the triple bond···I–C) *ca.* 177.76°, and one iodine···iodine type II interaction (Fig. 6b).

In the crystal structure of **D3**·H_2O, there are **D3**···**D3** water-bridged interactions (Fig. 7a) as well as direct **D3**···**D3** hydrogen bonds (Fig. 7b), and a triple bond···ethynyl hydrogen atom interaction *r*(C···centroid of the triple bond) *ca.* 3.87 Å, *θ*(centroid of the triple bond···H–C) *ca.* 138° (Fig. 7b).

Even though we were only able to determine the crystal structures of six co-crystals using single-crystal X-ray diffraction (Tables 3 and 4), the IR analysis of the sixteen attempted co-crystallizations found unambiguous evidence for co-crystal formation in each case (see the ESI†).

In the structure of **D1:A3**, there are two halogen bonds; I···N (a 20% combined vdW reduction) and I···O (a 16% vdW reduction). These interactions are mirrored by two hydrogen bonds, O···N and O···O, respectively, involving the same type of acceptor sites that participated in halogen bonds (Fig. 8).

The crystal structure of **D1:A4** displays the same set of intermolecular interactions as found in **D1:A3**: one I···N halogen bond (with a 22% vdW reduction) and one I···O halogen bond (with a 16% vdW reduction). Again, these interactions are mimicked by two hydrogen bonds, O···N and O···O, Table 3 and Fig. 9.

In the crystal structure of **D1:A5** we again find the same combination of two halogen bonds (with a 22% and a 17% reduction in the combined vdW radii for I···N and I···O, respectively) and two structurally similar hydrogen bonds (Fig. 10).

Up to this point, all three co-crystals of **D1** contain the same set of hydrogen and halogen bonds, but when acceptor **A3** is introduced to the geometric isomer **D2**, a different set of interactions are observed. The heteromeric co-crystallization is now driven only by two O···N hydrogen bonds, leaving the two C≡C–I moieties to form halogen bonds to the hydroxylic oxygen atoms (with a 15% vdW reduction) of the molecule to which they are attached (Fig. 11).

In the crystal structure of **D3:A3**, where the C≡C–I moieties have been replaced with C≡C–H groups on **D3**, O–H···N hydrogen bonds are exclusively responsible for co-crystal formation, accompanied by C≡C–H···O interactions involving the hydroxylic oxygen atoms of **D3** (Fig. 12).

Finally, in the crystal structure of **D3:A5**, a co-crystal is formed as a result of two O–H···N hydrogen bonds, and this time both ethynyl groups form hydrogen bonds with hydroxylic oxygen atoms as acceptor sites (Fig. 13).

Discussion

The crystal structure determination of the three target molecules revealed that both **D1** and **D3** appeared as hydrates in the solid state, whereas crystalline **D2** did not include any additional components. The inclusion of water molecules in structure **D1** makes it possible for C–I···O(hydroxyl) halogen bonds and

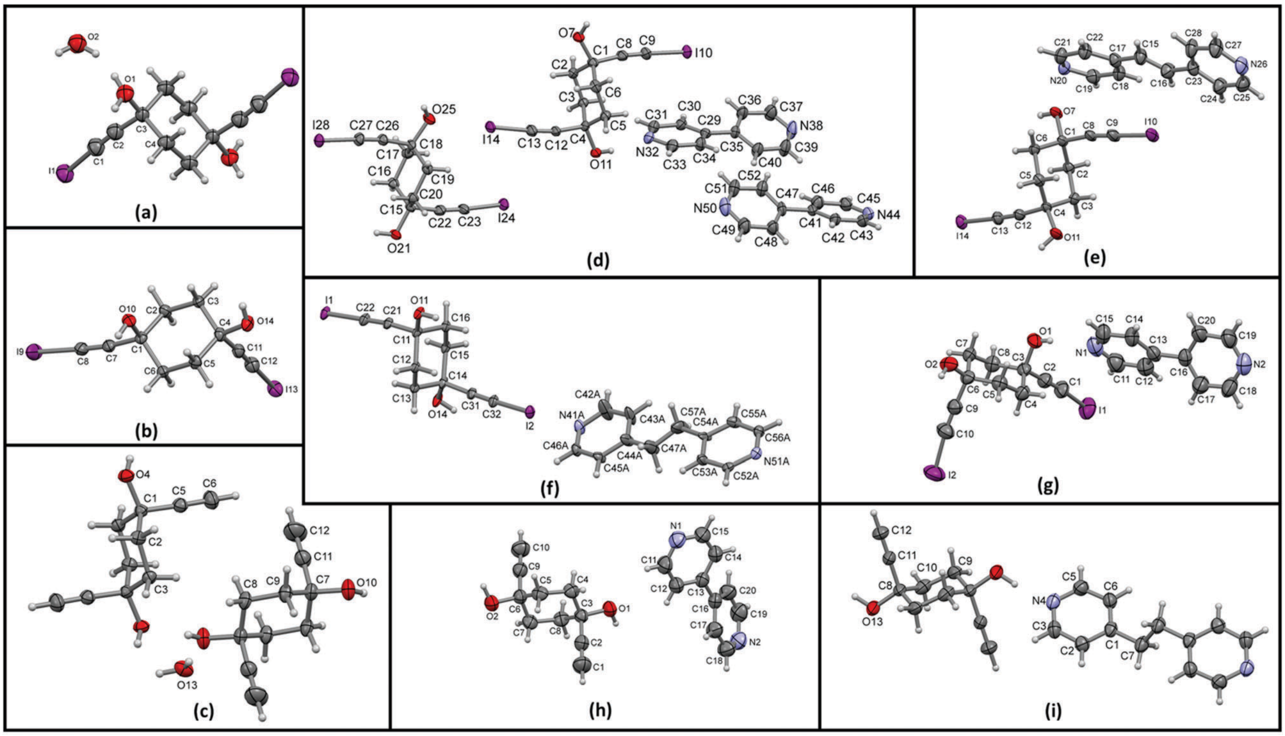

Fig. 4 ADPs for crystal structures (a) **D1**·H_2O, (b) **D2**, (c) **D3**·H_2O, (d) **D1**:**A3**, (e) **D1**:**A4**, (f) **D1**:**A5**, (g) **D2**:**A3**, (h) **D3**:**A3**, and (i) **D3**:**A5** (thermal ellipsoids of crystals are displayed at a 50% probability level).

Table 1 HB distances and angles in **D1–D3**

Compound	D–H···A	D···A (Å)	∠(DHA) (°)
D1·H_2O	O(1)–H(1O)···O(2)	2.8239(19)	164(8)
	O(2)–H(2O)···O(1)	2.8239(19)	154(8)
D2	O(10)–H(10)···O(14)	2.806(2)	173(3)
	O(14)–H(14)···O(10)	2.922(2)	170(3)
D3·H_2O	O(4)–H(4)···O(13)	2.6333(11)	173.2(16)
	O(10)–H(10)···O(4)	2.7789(11)	160.8(17)
	O(13)–H(13A)···O(10)	2.7575(13)	168.9(16)
	O(13)–H(13B)···O(4)	2.9174(12)	169.3(18)

Table 2 XB distances and angles in **D1–D2**

Compound	D–X···A	X···A (Å)	∠(DXA) (°)
D1·H_2O	C(1)–I(1)···O(1)	3.146(3)	174.68(15)
D2	C(8)–I(9)···I(13)	3.9222(4)	140.69(7)
	C(12)–I(13)···I(9)	3.9222(4)	71.49(7)
	C(12)–I(13)···C(8)	3.296(2)	168.69(8)
	C(12)–I(13)···C(7)	3.354(2)	170.34(8)

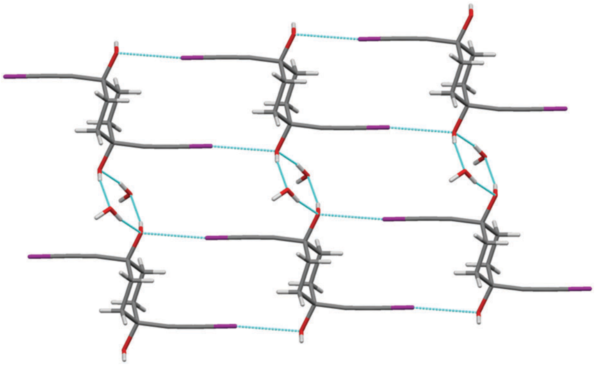

Fig. 5 Hydrogen bonding and halogen bonding in the crystal structure of **D1**·H_2O.

O–H···O(water) hydrogen bonds to exist side by side. The lack of water molecules in the structure of **D2** means that there is a shortage of oxygen acceptor sites and in this case, the competition between O–H and C–I leads to O–H···O hydrogen bonds. The C–I groups have to resort to forming type II halogen bonds to the electron-rich equatorial region of a neighboring iodine atom[41] and also through a side-on contact with a triple bond.[42] In the structure of **D3**·H_2O, the ethynyl hydrogen atoms also form hydrogen bonds through a side-on interaction with an electron rich area of the triple bond in an adjacent molecule of **D3**.[43]

IR spectroscopy is an effective and sensitive method for detecting co-crystal formation.[44] We observed a red shift of the O–H peak from *ca.* 3279 cm^{-1} to 3260 cm^{-1} with the formation of a co-crystal (**D1:A3**) and a red shift of the stretch associated with the triple bond (from *ca.* 2158 cm^{-1} to 2153 cm^{-1}). Complementary blue shifts of the acceptors in **D1:A3** were found (from *ca.* 1586 cm^{-1} to 1590 cm^{-1}) in 4,4′-bipyridine upon co-crystal formation.[45]

Based on the three co-crystals formed by **D1** with **A3–A5**, respectively, it seems that the XB and HB donors are equally capable of competing for the available acceptor sites even though they have different MEP values. The iodine atom acts in a structurally similar way to the hydrogen atom indicating the close competitiveness between the two and illustrating the

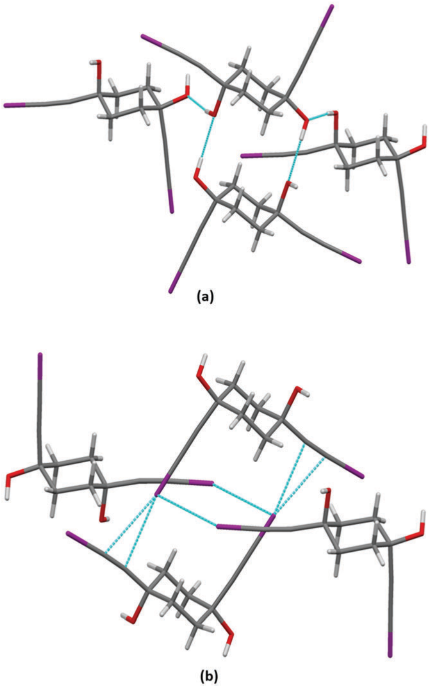

Fig. 6 Hydrogen bonds (a) and halogen bonds (b) in the crystal structure of **D2**.

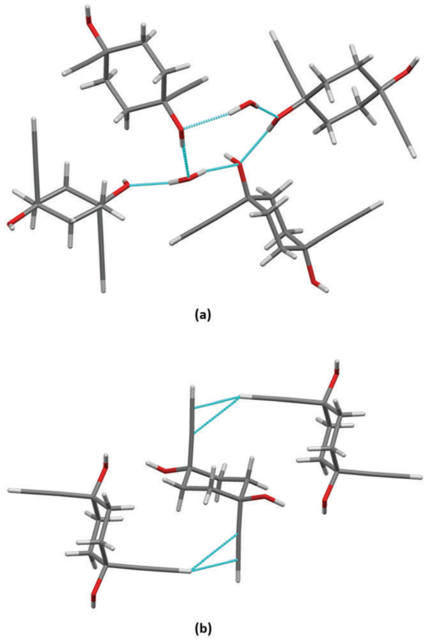

Fig. 7 (a) Water bridged hydrogen bonding and (b) C–H···C≡C hydrogen bond in the crystal structure of **D3**·H_2O.

difficulty in predicting the outcome solely based on MEP values.[46] It has been shown previously that if the Q value (Q = HB electrostatic potential – XB electrostatic potential)[31] is less than about 140 kJ mol^{-1} then the HB and XB donors are likely to be competitive with each other. In **D1** the difference in electrostatic potential between the two donors is 37 kJ mol^{-1} which is thus in agreement with earlier studies.

Table 3 HB distances and angles in the structures of six co-crystals

Compound	D–H···A	D···A (Å)	∠(DHA) (°)
D1:A3	O(7)–H(7)···O(11)	2.758(5)	159(9)
	O(11)–H(11)···N(32)	2.809(5)	161(7)
	O(21)–H(21)···N(44)	2.786(6)	163(7)
	O(25)–H(25)···O(21)	2.717(5)	171.5[a]
D1:A4	O(7)–H(7)···N(20)	2.792(3)	172(3)
	O(11)–H(11)···O(7)	2.740(2)	169(3)
D1:A5	O(11)–H(11)···N(51A)	2.726(7)	172.9[a]
	O(11)–H(11)···N(51B)	2.831(12)	174.7[a]
	O(14)–H(14)···O(11)	2.740(3)	168.7[a]
D2:A3	O(1)–H(1O)···N(1)	2.810(7)	165(9)
	O(11)–H(2O)···N(2)	2.791(7)	174(7)
D3:A3	O(1)–H(1O)···N(2)	2.7777(18)	170.5(19)
	O(2)–H(2O)···N(1)	2.8241(19)	170(2)
	C(10)–H(10)···O(1)	3.303(3)	173(2)
D3:A5	O(13)–H(13)···N(4)	2.7314(16)	171(2)
	C(12)–H(12)···O(13)	3.235(2)	160.7[a]

[a] Some of the hydrogen atoms involved in hydrogen bonding could not be located based on the difference electron density. Hence, they were placed in geometrically calculated positions and refined using a riding model.

Table 4 XB distances and angles in the structures of four co-crystals

Compound	D–X···A	X···A (Å)	∠(DXA) (°)
D1:A3	C(9)–I(10)···N(50)	2.826(5)	178.30(19)
	C(13)–I(14)···O(25)	2.938(4)	175.19(19)
	C(23)–I(24)···O(7)	2.951(4)	173.60(19)
	C(27)–I(28)···N(38)	2.782(4)	178.97(19)
D1:A4	C(9)–I(10)···O(11)	2.9273(17)	174.73(8)
	C(13)–I(14)···N(26)	2.768(2)	177.81(9)
D1:A5	C(32)–I(2)···N(41B)	2.755(8)	173.2(5)
	C(32)–I(2)···N(41A)	2.761(4)	179.9(2)
	C(22)–I(1)···O(14)	2.901(2)	175.12(9)
D2:A3	C(1)–I(1)···O(2)	2.978(4)	154.6(2)
	C(10)–I(2)···O(1)	2.955(4)	159.0(2)

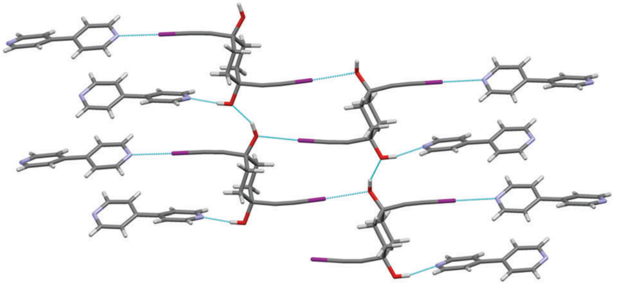

Fig. 8 Main HBs and XBs in the crystal structure of **D1**:**A3**.

Different relative positioning of the hydroxyl groups in **D2** compared to that in **D1** (equatorial:equatorial in **D1** *vs.* axial: equatorial in **D2**) (Fig. 1(a) and 2(b)) results in slightly different MEPs for hydrogen bond donors (axial OH; 224 kJ mol^{-1}, equatorial OH; 215 kJ mol^{-1}), making one hydroxyl group a better HB donor than the other. In contrast, even though the two iodine atoms in **D2** are in different geometric orientation (axial and equatorial), they show similar MEPs (187 kJ mol^{-1}). These different MEPs of the two O–H hydrogen bond donors are also reflected in the intermolecular bond distances in **D3:A3**, r(O axial···N) 2.791(7) Å and r(O equatorial···N) 2.810(7) Å

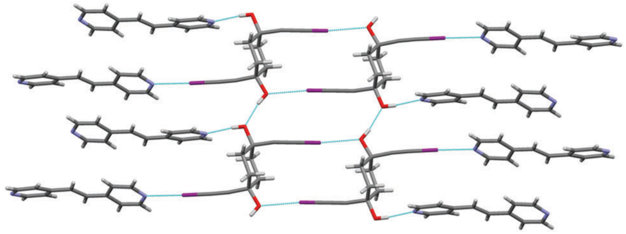

Fig. 9 Main HBs and XBs in the crystal structure of **D1**:**A4**.

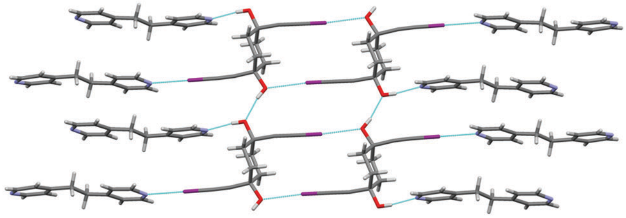

Fig. 10 Main HBs and XBs in the crystal structure of **D1**:**A5**.

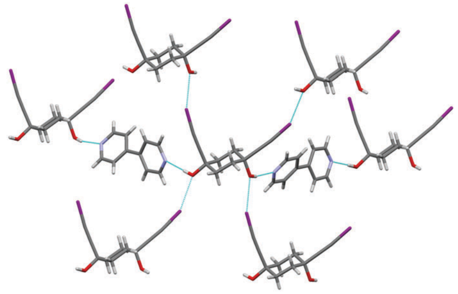

Fig. 11 Main HBs and XBs in the crystal structure of **D2**:**A3**.

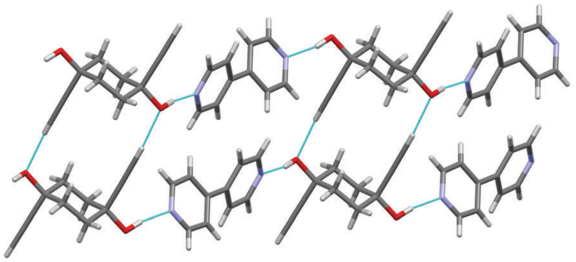

Fig. 12 Main HBs in the crystal structure of **D3**:**A3**.

(a high MEP value matches with a shorter bond distance, and *vice versa*). Even though the Q values of the two pairs of XB and HB donors on **D2** are 37 kJ mol^{-1} and 28 kJ mol^{-1}, respectively (substantially lower than 140 kJ mol^{-1}), the hydrogen-bond donors dominate over the C–I donors in the competition for the best hydrogen-bond acceptor, the hydroxylic oxygen atoms.

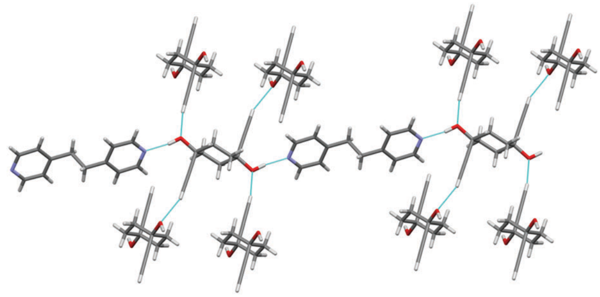

Fig. 13 Main HBs in the crystal structure of **D3**:**A5**.

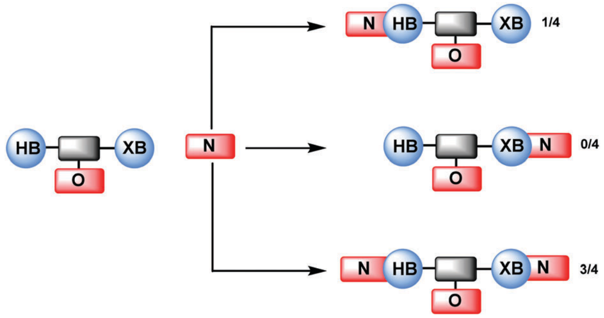

Scheme 6 Summary of interactions between HB/XB donors and nitrogen-based acceptors.

In the three co-crystals of **D1** (with **A3**, **A4**, and **A5**), both XB and HB donors act in comparable ways by each interacting with two nitrogen acceptor sites and two oxygen acceptors. In the one co-crystal of **D2** (which has a *cis*-configuration of donor sites) the HB donor drives the co-crystal synthesis by forming an O–H$\cdots$N hydrogen bond with bipyridine, which leaves the hydroxylic oxygen atoms to engage with the C–I halogen-bond donors indicating that relatively subtle changes in molecular geometry can tip the balance in favor of one donor over another (Scheme 6). Furthermore, the polarity of the solvent can also play a key role in shifting the balance between HB and XB interactions in a competitive situation.[24]

The intermolecular packing in **D1:A3** is different to that found in **D1:A4** and **D1:A5** due to the presence of additional moderate[47] to weak[48] $\pi\cdots\pi$ interactions ($r(\pi\cdots\pi)$ 3.83 Å and 3.94 Å) between the rings of **A3** (Fig. 14). In **D1:A4** and **D1:A5**, it is not possible for the pyridyl rings to stack on top of each other since the bridging groups between the rings in **A4** and **A5** necessitate that the aromatic groups end up being sandwiched between the aliphatic bridges of adjacent co-formers within each stack (Fig. 9 and 10), once the structure directing hydrogen and halogen bonds have formed.

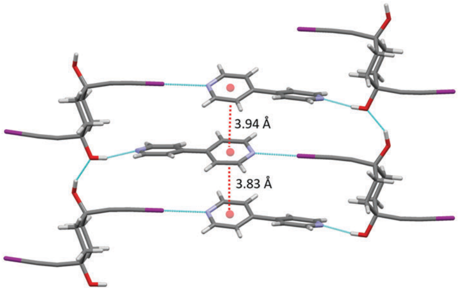

Fig. 14 Moderate/weak $\pi\cdots\pi$ stacking in the crystal structure of **D1**:**A3**.

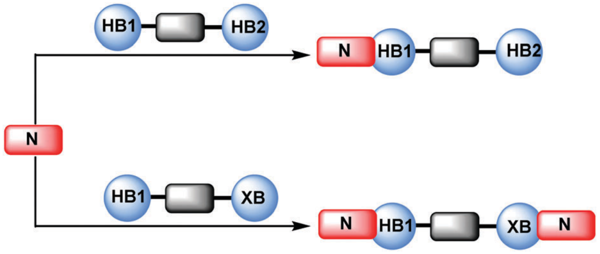

Scheme 7 Competition of halogen bonding with hydrogen bonding in the presence of the same acceptor.

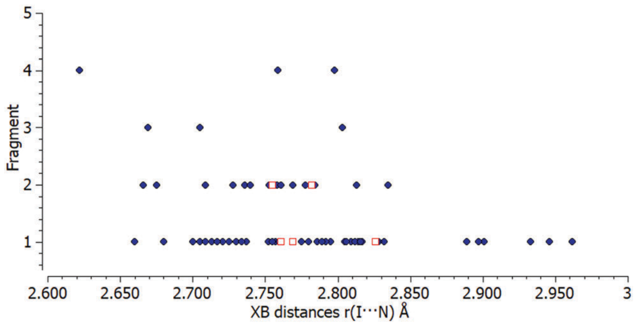

Fig. 15 XB distances between ethynyl iodine and aromatic nitrogen: reported in CSD (blue circles) and observed in this study (red hollow squares).

The ethynyl hydrogen atom is capable of making substantive hydrogen bonds with nitrogen based[49,50] or oxygen based[51] acceptors in co-crystallizations. However, in **D3** it cannot compete effectively with the hydroxyl hydrogen (Scheme 7) which indicates that the ethynyl hydrogen is a weaker donor than the ethynyl iodine.

Nitrogen acceptors of all co-crystals show a higher vdW reduction in XB bonding when compared to oxygen acceptors (average vdW radii reduction is 21% for I···N, average vdW reduction is 16% for I···O). All the XB distances and angles between aromatic nitrogen atoms and the ethynyl iodine functionality are in the range of values found among the 44 relevant structures found in the CSD[52] (Fig. 15 and 16). There is only one previously reported structure with an iodo-ethynyl halogen bond involving a hydroxyl oxygen atom *r*(I···O) *ca.*2.98 Å, (θ(C–I···O) *ca.*178.5°).[53]

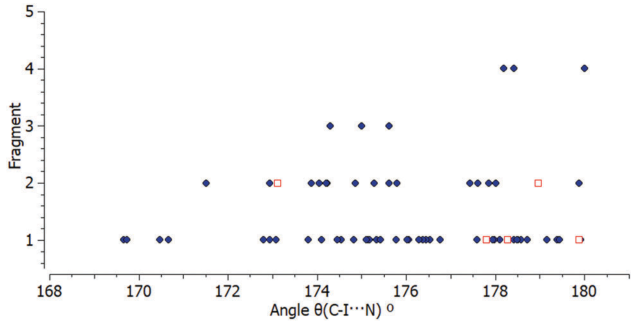

Fig. 16 XB angles θ(C–I···N): reported in CSD (blue circles) and observed in this study (red hollow squares).

The angular dependence of halogen bonds shows a greater tendency towards linearity when nitrogen acceptors are involved (average θ(C–I···N) *ca.*178°), compared to when oxygen atoms act as acceptor sites (average θ(C–I···O) *ca.*169°).

Conclusions

Based on the structural information on two HB/XB tetrafunctionalized molecules, as well as four co-crystals thereof, it is clear that the ability of R–O–H hydrogen bond donors and R–C≡C–I halogen bond donors to engage in structure-directing interactions is very finely balanced. By and large, the hydroxylic groups and the iodo-ethynyl groups are equally successful when competing for a limited number of nitrogen-based or oxygen-based acceptor sites. The fact that *trans*-1,4-bis(iodoethynyl)cyclohexane-1,4-diol, **D1**, and *cis*-1,4-bis(iodoethynyl)cyclohexane-1,4-diol, **D2**, behave differently does however, indicate that the balance between hydrogen and halogen bonds can be altered by very small changes in the molecular conformation. In the control molecule, *trans*-1,4-diethynylcyclohexane-1,4-diol, **D3**, where the activated XB donor was replaced by a relatively weak HB donor, R–C≡C–H, the hydroxylic moiety is now dominant due to its substantially larger positive electrostatic potential on the proton. The differences in electrostatic potential values of the HB and XB donors provide a useful indication of how the balance between the competing forces will manifest itself in the resulting crystal structure. The structural information presented in this study, coupled with rationalizations of the observed results against a background of calculated molecular electrostatic potentials, may facilitate the reliable design and synthesis of multi-component solid-state architectures using a transferable synthetic protocol based on a variety of intermolecular interactions.

Conflicts of interest

There are no conflicts to declare.

Acknowledgements

This material is based on the work supported by, or in part by, the U. S. Army Research Laboratory and the U. S. Army Research Office under contract/grant number W911NF-13-1-0387 (to C. B. A. and J. C. G.) and by the Croatian Science Foundation under project UIP-11-2013-1809 (to M. D.). We are also grateful to Dr V. Day (University of Kansas) for collecting some single-crystal X-ray data.

References

1 C. B. Aakeröy and P. D. Chopade, Cocrystals: Synthesis, Structure, and Applications, in *Supramolecular Chemistry*, John Wiley & Sons, Ltd, 2012.
2 C. Rest, R. Kandanelli and G. Fernandez, *Chem. Soc. Rev.*, 2015, **44**, 2543–2572.
3 M. J. Webber, E. A. Appel, E. W. Meijer and R. Langer, *Nat. Mater.*, 2016, **15**, 13–26.

4 C. B. Aakeröy, P. D. Chopade and J. Desper, *Cryst. Growth Des.*, 2011, **11**, 5333–5336.

5 H. R. Khavasi and A. A. Tehrani, *CrystEngComm*, 2013, **15**, 5813–5820.

6 D. A. Adsmond, A. S. Sinha, U. B. R. Khandavilli, A. R. Maguire and S. E. Lawrence, *Cryst. Growth Des.*, 2016, **16**, 59–69.

7 T. Shirman, M. Boterashvili, M. Orbach, D. Freeman, L. J. W. Shimon, M. Lahav and M. E. van der Boom, *Cryst. Growth Des.*, 2015, **15**, 4756–4759.

8 H. R. Khavasi and M. Esmaeili, *CrystEngComm*, 2014, **16**, 8479–8485.

9 P. Gómez, M. Más-Montoya, I. da Silva, J. P. Cerón-Carrasco, A. Tárraga and D. Curiel, *Cryst. Growth Des.*, 2017, **17**, 3371–3378.

10 X. Li, Y. Gao, R. Harniman, M. Winnik and I. Manners, *J. Am. Chem. Soc.*, 2016, **138**, 12902–12912.

11 Z. Gao, Y. Han, S. Chen, Z. Li, H. Tong and F. Wang, *ACS Macro Lett.*, 2017, **6**, 541–545.

12 H. Wang, Z. Bao, H. Wu, R.-B. Lin, W. Zhou, T.-L. Hu, B. Li, J. C.-G. Zhao and B. Chen, *Chem. Commun.*, 2017, **53**, 11150–11153.

13 A. Priimagi, G. Cavallo, P. Metrangolo and G. Resnati, *Acc. Chem. Res.*, 2013, **46**, 2686–2695.

14 M. C. Pfrunder, A. S. Micallef, L. Rintoul, D. P. Arnold and J. McMurtrie, *Cryst. Growth Des.*, 2016, **16**, 681–695.

15 R. Liu, H. Wang and W. J. Jin, *Cryst. Growth Des.*, 2017, **17**, 3331–3337.

16 J. C. Gamekkanda, A. S. Sinha, J. Desper, M. Đaković and C. B. Aakeröy, *Crystals*, 2017, **7**, 226.

17 D. Yan, D.-K. Bučar, A. Delori, B. Patel, G. O. Lloyd, W. Jones and X. Duan, *Chem. – Eur. J.*, 2013, **19**, 8213–8219.

18 A. Vanderkooy and M. S. Taylor, *Faraday Discuss.*, 2017, **203**, 285–299.

19 C. B. Aakeröy, T. K. Wijethunga, J. Desper and M. Đaković, *Cryst. Growth Des.*, 2016, **16**, 2662–2670.

20 T. Clark, *Faraday Discuss.*, 2017, **203**, 9–27.

21 M. D. Perera, J. Desper, A. S. Sinha and C. B. Aakeröy, *CrystEngComm*, 2016, **18**, 8631–8636.

22 R. K. Rowe and P. S. Ho, *Acta Crystallogr., Sect. B: Struct. Sci., Cryst. Eng. Mater.*, 2017, **73**, 255–264.

23 C. A. Gunawardana, J. Desper, A. S. Sinha, M. Đaković and C. B. Aakeröy, *Faraday Discuss.*, 2017, **203**, 371–388.

24 C. C. Robertson, J. S. Wright, E. J. Carrington, R. N. Perutz, C. A. Hunter and L. Brammer, *Chem. Sci.*, 2017, **8**, 5392–5398.

25 I. D. H. Oswald, W. D. S. Motherwell and S. Parsons, *Acta Crystallogr., Sect. B: Struct. Sci.*, 2005, **61**, 46–57.

26 R. B. Walsh, C. W. Padgett, P. Metrangolo, G. Resnati, T. W. Hanks and W. T. Pennington, *Cryst. Growth Des.*, 2001, **1**, 165–175.

27 E. Corradi, S. V. Meille, M. T. Messina, P. Metrangolo and G. Resnati, *Angew. Chem., Int. Ed.*, 2000, **39**, 1782–1786.

28 J.-L. Syssa-Magale, K. Boubekeur, P. Palvadeau, A. Meerschaut and B. Schollhorn, *CrystEngComm*, 2005, **7**, 302–308.

29 D. R. Weyna, T. Shattock, P. Vishweshwar and M. J. Zaworotko, *Cryst. Growth Des.*, 2009, **9**, 1106–1123.

30 C. B. Aakeröy, D. Welideniya and J. Desper, *CrystEngComm*, 2017, **19**, 11–13.

31 C. B. Aakeröy, C. L. Spartz, S. Dembowski, S. Dwyre and J. Desper, *IUCrJ*, 2015, **2**, 498–510.

32 R. Montis, M. Arca, M. C. Aragoni, A. Bauza, F. Demartin, A. Frontera, F. Isaia and V. Lippolis, *CrystEngComm*, 2017, **19**, 4401–4412.

33 Y. Geboes, F. De Proft and W. A. Herrebout, *Acta Crystallogr., Sect. B: Struct. Sci., Cryst. Eng. Mater.*, 2017, **73**, 168–178.

34 H. Ding, Y. Lu, W. Wu and H. Liu, *Chem. Phys.*, 2014, **441**, 30–37.

35 C. B. Aakeröy, S. Panikkattu, P. D. Chopade and J. Desper, *CrystEngComm*, 2013, **15**, 3125–3136.

36 O. Dumele, D. Wu, N. Trapp, N. Goroff and F. Diederich, *Org. Lett.*, 2014, **16**, 4722–4725.

37 C. B. Aakeröy, T. K. Wijethunga, J. Desper and M. Đaković, *Cryst. Growth Des.*, 2015, **15**, 3853–3861.

38 N. R. Goud, O. Bolton, E. C. Burgess and A. J. Matzger, *Cryst. Growth Des.*, 2016, **16**, 1765–1771.

39 *Spartan'14 Wavefunction*, Inc., Irvine., 2013.

40 R. Hosseinzadeh, M. K. Abolfazli, M. Mohseni, M. Mohadjerani and Z. Lasemi, *J. Heterocycl. Chem.*, 2014, **51**, 1298–1305.

41 G. Cavallo, P. Metrangolo, R. Milani, T. Pilati, A. Priimagi, G. Resnati and G. Terraneo, *Chem. Rev.*, 2016, **116**, 2478–2601.

42 A. Mukherjee, S. Tothadi and G. R. Desiraju, *Acc. Chem. Res.*, 2014, **47**, 2514–2524.

43 T. Steiner, *J. Chem. Soc., Chem. Commun.*, 1995, 95–96.

44 J. Joseph and E. D. Jemmis, *J. Am. Chem. Soc.*, 2007, **129**, 4620–4632.

45 L. González, N. Gimeno, R. M. Tejedor, V. Polo, M. B. Ros, S. Uriel and J. L. Serrano, *Chem. Mater.*, 2013, **25**, 4503–4510.

46 M. K. Corpinot, S. A. Stratford, M. Arhangelskis, J. Anka-Lufford, I. Halasz, N. Judas, W. Jones and D.-K. Bucar, *CrystEngComm*, 2016, **18**, 5434–5439.

47 M. Moradi, L. G. Tulli, J. Nowakowski, M. Baljozovic, T. A. Jung and P. Shahgaldian, *Angew. Chem., Int. Ed.*, 2017, **56**, 14395–14399.

48 I. Avasthi, S. Khanna, S. K. Tripathi and S. Verma, *CrystEngComm*, 2017, **19**, 5202–5213.

49 E. Bosch, N. P. Bowling and J. Darko, *Cryst. Growth Des.*, 2015, **15**, 1634–1641.

50 E. Bosch, *Cryst. Growth Des.*, 2010, **10**, 3808–3813.

51 E. Bosch, *Acta Crystallogr., Sect. C: Struct. Chem.*, 2016, **72**, 748–752.

52 C. R. Groom, I. J. Bruno, M. P. Lightfoot and S. C. Ward, *Acta Crystallogr., Sect. B: Struct. Sci., Cryst. Eng. Mater.*, 2016, **72**, 171–179.

53 D. K. Moss, J. D. Spence and M. H. Nantz, *J. Org. Chem.*, 1999, **64**, 4339–4343.